Published as: *Curr Biol*. 2007 October 23; 17(20): 1752–1758.

Role of septin cytoskeleton in spine morphogenesis and dendrite development in neurons

Tomoko Tada[1], **Alyson Simonetta**[1], **Matthew Batterton**[1], **Makoto Kinoshita**[2], **Dieter Edbauer**[1], and **Morgan Sheng**[1,*]

1 *The Picower Institute for Learning and Memory, RIKEN-MIT Neuroscience Research Center, Howard Hughes Medical Institute, Massachusetts Institute of Technology, Cambridge, MA 02446, USA*

2 *Biochemistry and Cell Biology Unit, HMRO, Kyoto University Graduate School of Medicine, Yoshida Konoe, Sakyo, Kyoto 606-8501, Japan*

Summary

Septins are GTP-binding proteins that polymerize into heteromeric filaments and form microscopic bundles or ring structures *in vitro* and *in vivo*. Because of these properties and their ability to associate with membrane, F-actin and microtubules, septins have been generally regarded as cytoskeletal components [1,2]. Septins are known to play roles in cytokinesis, membrane trafficking and as structural scaffolds; however, their function in neurons is poorly understood. Many members of the septin family, including Septin7 (Sept7), were found by mass spectrometry analysis of postsynaptic density (PSD) fractions of the brain [3,4], suggesting a possible postsynaptic function of septins in neurons. We report that Sept7 is localized at the base of dendritic protrusions and at dendritic branch points in cultured hippocampal neurons -- a distribution reminiscent of septin localization in the bud neck of budding yeast. Overexpression of Sept7 increased dendrite branching and the density of dendritic protrusions, while RNA interference (RNAi) mediated knockdown of Sept7 led to reduced dendrite arborization and a higher proportion of immature protrusions. These data suggest that Sept7 is critical for spine morphogenesis and dendrite development during neuronal maturation.

Keywords

dendrite branching; dendritic protrusion; dendritic spine; spine dynamics

Results and discussion

Expression pattern of septin family in the rat brain and neuron culture

Nine of the 14 septins in mammals (Sept2, 3, 4, 5, 6, 7, 8, 9 and 11) have been found in rat brain PSD fractions by mass spectrometry [3–5] (Human Sept14, GenBank accession No. NP_997249), of which Sept7 appeared to be the most abundant [3]. Immunoblotting of rat brain fractions confirmed that Sept2, 5, 6, 7 and 11 were enriched in Triton X-100 extracted PSD fractions (PSDI and PSDII) compared with P2 crude synaptosomal fraction (Fig. 1A). However, unlike PSD-95, all the tested septins were largely extracted from the PSD fraction

* Corresponding author: Morgan Sheng, The Picower Institute for Learning and Memory, Massachusetts Institute of Technology, 77 Massachusetts Ave (46-4303A), Cambridge, MA 02139. msheng@mit.edu, Phone 617.452.3716; Fax 617.452.3692.

with the stronger detergent sarkosyl (PSDIII), suggesting that septins are not "core" components of PSD (Fig. 1A).

By immunoblotting, septins were widely expressed in the rat CNS, though with non-identical patterns (Fig. 1B). For instance, Sept5 and Sept6 were more highly expressed in cortex and hippocampus than in cerebellum, whereas Sept11 was more abundant in cerebellum and spinal cord than in forebrain. The levels of Sept2, 5, 6, 7 gradually increased during development of the brain from late embryonic stages (E15) through postnatal day 7 (P7) to adult (P45) throughout the brain (Fig. 1B and 1C). Sept4 was mainly expressed in adult brain (Fig. 1B and 1C). In contrast, Sept11 expression decreased from P7 to adult in cerebellum and spinal cord, and remained relatively unchanged during this time span in cortex, hippocampus and striatum (Fig. 1B and 1C). The expression of the different septin proteins generally showed an upward trend during development of hippocampal neurons in dissociated culture (1–4 weeks in vitro; Fig. 1D).

Endogenous Sept7 localized at the base of protrusions

The septin family in mammals can be classified into four paralogous groups by amino acid sequence homology: Sept2 group (Sept1, 2, 4, 5), Sept3 group (Sept3, 9 12), Sept6 group (Sept6, 8, 10, 11, 14), Sept7 group (Sept7, 13) [5–7]. Sept7 is the predominant member of its classification group in neurons, since Sept13 is modestly expressed in brain [5]. Sept7 is broadly expressed in the brain [8] and appears to be the most abundant septin in adult rat forebrain PSD fractions by semi-quantitative mass spectrometry analysis [3]. We focused on Sept7 because Sept7 seems to be a core component of most multimeric septin complexes [1], and because of the availability of a high quality antibody for immunostaining. In very young neurons (DIV3), endogenous Sept7 localized in the growth cones of dendritic processes extending from the cell soma (Supplementary Fig. 1A, 1B arrowheads, 1D) and in fine puncta at the base of axonal protrusions (Supplementary Fig. 1A, 1C arrowheads, 1E). PSD-95 was expressed in the cell body and dendritic growth cones at DIV3 (Supplementary Fig. 1A3, 1B3). At 7 days in vitro (DIV7), endogenous Sept7 formed clusters in the dendrite, many of which were located at the base of filopodia-like dendritic protrusions (Fig. 2B–D, arrowheads) and at the branch points of dendrites (Fig. 2D arrows). Extensions from dendrites shorter than 10 μm were defined as dendritic protrusions and those longer than 10 μm were defined as dendrite branches. There was no significant colocalization between endogenous Sept7 and PSD-95 puncta in the dendrite at DIV7 (Fig. 2B). At DIV14, endogenous Sept7 localized in numerous puncta of various sizes and shapes in both dendrites and axons (Supplementary Fig. 1F1 and 1G1). Some of the endogenous Sept7 puncta localized at the base of dendritic spines stained with the postsynaptic marker PSD-95 (Supplementary Fig. 1F, 1G arrowheads, 1H arrowheads). In addition to the punctate staining within dendrites, a large number of Sept7 puncta lay "outside" of the dendrite, often apposed to PSD-95-positive dendritic spines (Supplemental Fig. 1G4, 1H arrows). We interpret these clusters to represent glia, axons or presynaptic terminals. The latter is consistent with previous light and electron microscopic observations of Sept7 located beneath the presynaptic membrane [8].

To confirm the antibody specificity, we knocked down Sept7 with specific shRNA and found that Sept7 immunostaining was strongly reduced along the dendrites of transfected neurons (Supplementary Fig. 2C–F). Transfected EGFP-Sept7 and FLAG-Sept7 showed a similar clustered dendritic localization as endogenous Sept7 (data not shown), supporting the conclusion that Sept7 specifically targets to the base of dendritic protrusions. Endogenous Sept7 was highly colocalized with endogenous Sept5 in cultured hippocampal neurons, consistent with these septins forming heteromeric polymers (Fig. 2E and 2F, arrowheads).

The clustering of Sept7 at the base of dendritic protrusions is reminiscent of the septin localization at the bud neck in budding yeast, where it forms hourglass and ring structures

during cytokinesis [9–11]. However, we were unable to observe either hourglass or ring-like structures of endogenous or transfected Sept7 at the base of dendritic protrusions. The dimensions of the septin ring in dendrites might be beyond the resolution of our confocal microscopy. Dendritic Sept7 could also exist in one of the other higher-order structures reported before, such as arc [1] or gauze [12].

Septin overexpression increased dendrite branching and protrusion density

We hypothesized that Sept7 located at the base of dendritic protrusions played a role in the formation and/or growth of these bud-like compartments. During the first 1–2 weeks in culture, neuronal dendrites mainly display numerous long thin filopodia-like protrusions, which gradually develop into or are replaced by mature spines with defined heads [13–18]. To examine septin function in protrusion and dendrite development, we first performed overexpression studies in young cultures (Fig. 3). Cultured hippocampal neurons were transfected at DIV7 with FLAG-tagged Sept2, 6 or 7. Five days later, they were fixed and their morphology was visualized by cotransfected EGFP. Overexpression of these septins did not affect the mean length or head width of protrusions (Fig. 3B and 3C). Overexpression of Sept2, 6 or 7 increased the density of dendritic protrusions by ~25–30%, compared with control neurons transfected with the parental FLAG epitope vector and EGFP (Fig. 3D). Overexpression of Sept2, 6 or 7 also increased dendrite complexity, as measured by Sholl analysis, which counts the number of intersections made by dendrites with concentric circles of increasing distance from the cell body (Fig. 3E). In addition, the total number of dendrite branch-ends was elevated (Fig. 3F), confirming that dendrite branching was enhanced by septin overexpression. Overall the phenotype of Sept2, 6 and 7 overexpression was very similar.

Septin knockdown impairs spine and dendrite development

To study the loss-of-function phenotype, we turned to RNA interference (RNAi). Specific shRNA-expressing constructs targeting Sept2, 5, 6 or 7 were generated that caused >90% knockdown of their cognate EGFP-tagged septin when cotransfected in HEK293 cells (Supplemental Fig. 2A) or in neurons (Supplemental Fig. 2B). None of the RNAi constructs severely suppressed expression of other septin family members tested (Supplementary Fig. 2A and 2B). Endogenous Sept5 and Sept7 immunostaining in neurons were reduced to ~40% of pSuper control by their specific RNAi constructs (Supplementary Fig. 2C–F). We were unable to test the efficacy of knockdown of endogenous Sept2 and 6, because our antibodies did not provide convincing immunostaining in neurons.

We analyzed the effect of knockdown of specific septins on the morphogenesis of dendritic protrusions and dendrites at five days after transfection (DIV7+5), as in the overexpression experiments above. Neuronal morphology was visualized by cotransfected β-galactosidase. Empty vector pSuper and control RNAi constructs targeting the zinc transporter ZnT3 or EGFP did not affect spine morphology. Knockdown of Sept2 did not alter spine size, but caused a significant reduction in protrusion density (Fig. 4A–D). Knockdown of Sept5 did not significantly change the morphology of dendritic protrusions, but there was a tendency to decreased protrusion density (Fig. 4A–D). Knockdown of Sept6 significantly reduced protrusion density, and the remaining protrusions were on average slightly longer and wider (Fig. 4A–D). Some of the protrusions in Sept6 RNAi neurons showed abnormally branched and “spread” morphology of the spine head (Fig. 4A). Of the septin genes tested, only Sept7 knockdown did not cause reduction in protrusion density; however, in Sept7 RNAi transfected neurons, there was a relatively high density of long filopodia-like protrusions (Fig. 4A–D), resulting in markedly increased mean protrusion length (Fig. 4B). The effect of Sept7 RNAi on protrusion morphology was rescued by coexpression of an RNAi-resistant cDNA of Sept7 (Fig. 4A–D; Sept7 RNAi+Sept7*; and Supplemental Fig 3B), but not by coexpression of an unrelated cDNA (mCherry; data not shown), confirming the specificity of the Sept7 RNAi

phenotype. Overall the septin RNAi data suggest that septins are important for the morphogenesis of normal mature spines in developing neurons and imply some differences in function or expression among septin isoforms.

By Sholl analysis, we found that knockdown of Sept2, 5, 6 or 7 all strongly impaired dendrite complexity (Fig. 4E and 4F), resulting in a reduction of total branch ends (Fig. 4G). The negative effect of Sept5 RNAi and Sept7 RNAi on dendrite complexity and branching were significantly rescued by coexpression of RNAi-resistant cDNAs of Sept5 and Sept7, respectively, but completely unaffected by coexpression of mCherry (Fig. 4F and 4G and Supplementary Fig. 3B–D). These data support the specificity of the phenotype of septin knockdown. Together with the increased dendrite complexity found upon septin overexpression, our results indicate that one function of septins is to promote dendrite branching.

Consistent with previous reports of presynaptic localization of Sept7 [8], we found endogenous Sept7 to be present in axons and concentrated in clusters apposed to dendritic protrusions in DIV14 cultured hippocampal neurons (Supplementary Fig. 1F–H arrows). In addition, however, we describe here a previously unknown punctate distribution of Sept7 within dendrites – at the base of dendritic protrusions and at dendritic branch points. This dendritic pattern of Sept7 was particularly obvious in young neurons (DIV7) when synapses are fewer, and therefore the “presynaptic” pattern of Sept7 distribution is less prominent (Fig. 2). Transfected EGFP-Sept7 and FLAG-Sept7 showed a similar clustered dendritic localization as endogenous Sept7 (data not shown), and RNAi knockdown of Sept7 reduced Sept7 punctate staining along dendrites (Supplementary Fig. 2D–F), supporting the conclusion that Sept7 specifically targets to the base of dendritic protrusions.

The clustering of Sept7 at the base of dendritic protrusions is reminiscent of septin localization at the bud neck in budding yeast. At the bud neck, the yeast septin assembly acts as a scaffold for the proper localization of a variety of proteins, including those involved in mitotic spindle positioning [19–21], cell cycle progression [22–24], and cell wall synthesis [25,26]. Since the development of spines and branches from the dendritic shaft depends on polarized membrane growth, we speculate that neural septins play a role analogous to yeast septins, promoting polarized transport of membrane and proteins into extending protrusions or incipient branches. In yeast, the septin ring at the bud neck also acts as a “diffusion barrier” to compartmentalize and separate the mother and daughter cells [27,28]. The surface of neuronal dendrites shows prominent physical and functional compartmentalization between dendritic shaft and spines [29–33]. It is uncertain what types of diffusion barriers exist between the dendritic shaft and dendritic spines, or between the main dendritic trunk and new dendritic branches, but such diffusion barriers would promote the molecular differentiation and the stability and growth of dendritic spines and dendritic branches.

Filopodia on dendrites can develop into nascent dendrite branches as well as dendritic spines [13–18]. We hypothesize that septins act as a diffusion barrier at the base of the protrusion that prevents the “leakage” of spine/branch constituents back into the dendritic shaft. In this way, septins would promote the growth/maturation and stability of developing protrusions that eventually lead to mature spines and dendritic branches. Consistent with this hypothesis, overexpression of septins enhances, whereas RNAi of septins reduces, the branching of dendrites and the density of protrusions. The apparent exception is knockdown of Sept7, which does not decrease total protrusion density but causes the appearance of many thin filopodia-like protrusions. The Sept7 loss-of-function phenotype could result from impaired targeting into developing protrusions of proteins required for spine maturation, or might be a secondary response to loss of mature spines.

Experimental Procedures

DNA constructs

See Supplemental Table 1.

RNA interference in hippocampal neurons

For RNAi target sequences, see Supplementary Table 2.

Antibodies

Mouse monoclonal PSD-95 K28/43 was a gift from J. Trimmer, UC Davis. All of the polyclonal septin antibodies (Sept2, 4, 5, 6, 7 and 11 antibodies) were raised against synthetic peptides of the respective septin and affinity-purified (Supplementaly Table 3). The following antibodies were purchased from commercial sources: monoclonal mouse EGFP 3E6 (Qbiogene, Inc), polyclonal rabbit EGFP (MBL), polyclonal rabbit β-galactosidase (IPN/Cappel), monoclonal mouse FLAG M2 (Sigma), monoclonal mouse Bassoon (Sigma), polyclonal rabbit RFP (US Biological), monoclonal mouse α-Tubulin B-5-1-2 (Sigma), monoclonal mouse β-Actin AC-15 (Abcam), anti-mouse, anti-rabbit and anti-guinea pig Alexa 488- and 568-conjugated secondary antibodies (Molecular Probes), Alexa 488-phalloidin (Molecular Probes), Cy3- and Cy5-conjugated secondary antibodies (Jackson ImmunoResearch Labs), and mouse, rabbit, and guinea pig HRP linked IgG (Amersham Biosciences).

Hippocampal Cultures, Transfection, and Immunostaining

Hippocampal neurons were prepared from embryonic day 19 Sprague-Dawley rats and plated on glass coverslips coated with 37.5 μg/ml poly-D-lysine and 2.5 μg/ml laminin. Cultures were grown in Neurobasal medium (Invitrogen) containing 2% B27 (Invitrogen), 0.5 mM glutamine (Invitrogen), 12.5 μM glutamate (Sigma), and 1% penicillin/streptomycin (Invitrogen). Neurons were transfected at DIV7 with Lipofectamine 2000 (Invitrogen). The following DNA ratios were used: 1:2 (EGFP:FLAG-septin) for septin overexpression (Fig. 3); 2:3 (β-galactosidase:Septin RNAi) for RNAi against septin (Fig. 4, Supplemental Fig. 2 and 3); 2:1:4 (β-galactosidase:Septin RNAi:FLAG-septin*) for rescue of septin RNAi (Fig. 4 and Supplemental Fig. 3). After 5 days transfection (DIV7+5), neurons were fixed in PBS (pH 7.4) containing 4% formaldehyde and 4% sucrose, for 10 min at room temperature. In immunostaining, primary antibodies were applied overnight at 4°C, and secondary antibodies were applied for 1 hour at room temperature, as previously described [34].

Image Acquisition and Quantitation

Confocal images of neurons were obtained using a Zeiss 63x (NA 1.4; for spine morphology) or Zeiss 40x objectives (NA 1.3; for Sholl analysis and branch end counting) with sequential acquisition settings at the resolution of the confocal (1024 × 1024 pixels). Each image is a composite constructed from a series of images taken throughout the z aspect of each cell. The parameters of each composite image are optimized for the particular lens and pinhole setting. The confocal microscope settings were kept the same for all scans in each experiment. Morphometric analysis and quantification were done using MetaMorph image analysis software (Universal Imaging). For spine morphology studies, individual dendritic protrusions were manually traced, and the maximum length and head width of each dendritic protrusions were measured by MetaMorph software and logged into Microsoft Excel, as previously described [34]. For Sholl analysis, concentric circles with 12.5 μm differences in diameter were drawn around the cell body, and the number of dendrites crossing each circle was manually counted. For dendrite tip number, tips of all dendritic protrusions >10 μm were manually counted. The number of neurons used for quantification is indicated in the figure legends. Acquisition of microscopy images and morphometric quantification were performed by

investigators blind to the experimental condition. For quantification of septin shRNA effects on the fluorescence level of EGFP-tagged or endogenous septin immunostaining in transfected neurons, cell images were collected using identical intensity settings in each experiment. We randomly selected cells and manually traced the dendrites of transfected neurons, and measured the average EGFP or endogenous septin immunostaining fluorescence intensity expressed in arbitrary units of fluorescence per square area for the traced regions by MetaMorph software (Supplemental Fig. 2B, 2C).

PSD Fractionation

PSD fractions were prepared from adult rat forebrains as previously described [3]. Briefly, synaptosomes were purified from crude membrane fraction (P2) by discontinuous sucrose density gradient centrifugation. To obtain PSD fractions, synaptosomes were extracted once (PSDI) or twice (PSDII) with 0.5% Triton X-100, or extracted with 0.5% Triton X-100 followed by 3% sarkosyl (PSDIII).

Supplementary Material

Refer to Web version on PubMed Central for supplementary material.

Acknowledgements

We are grateful to Dr. Roger Y. Tsien for mCherry cDNA, Dr. Jacek Jaworski for the plasmid pSuper-EGFP shRNA. Funding for the authors' research came from the National Institutes of Health (MH076936) and RIKEN-MIT Neuroscience Research Center. M.S. is Investigator of the Howard Hughes Medical Institute. T.T. is supported in part by a fellowship of Yamanouchi Foundation for Research on Metabolic Disorders. D.E. was supported by Emmy Noether fellowship of Deutsche Forschungsgemeinschaft.

References

1. Kinoshita M, Field CM, Coughlin ML, Straight AF, Mitchison TJ. Self- and actin-templated assembly of Mammalian septins. Dev Cell 2002;3:791–802. [PubMed: 12479805]
2. Kinoshita M. Diversity of septin scaffolds. Curr Opin Cell Biol 2006;18:54–60. [PubMed: 16356703]
3. Peng J, Kim MJ, Cheng D, Duong DM, Gygi SP, Sheng M. Semiquantitative proteomic analysis of rat forebrain postsynaptic density fractions by mass spectrometry. J Biol Chem 2004;279:21003–21011. [PubMed: 15020595]
4. Collins MO, Husi H, Yu L, Brandon JM, Anderson CN, Blackstock WP, Choudhary JS, Grant SG. Molecular characterization and comparison of the components and multiprotein complexes in the postsynaptic proteome. J Neurochem. 2005
5. Hall PA, Jung K, Hillan KJ, Russell SE. Expression profiling the human septin gene family. J Pathol 2005;206:269–278. [PubMed: 15915442]
6. Kartmann B, Roth D. Novel roles for mammalian septins: from vesicle trafficking to oncogenesis. J Cell Sci 2001;114:839–844. [PubMed: 11181167]
7. Spiliotis ET, Kinoshita M, Nelson WJ. A mitotic septin scaffold required for Mammalian chromosome congression and segregation. Science 2005;307:1781–1785. [PubMed: 15774761]
8. Kinoshita A, Noda M, Kinoshita M. Differential localization of septins in the mouse brain. J Comp Neurol 2000;428:223–239. [PubMed: 11064363]
9. Longtine MS, Bi E. Regulation of septin organization and function in yeast. Trends Cell Biol 2003;13:403–409. [PubMed: 12888292]
10. Vrabioiu AM, Mitchison TJ. Structural insights into yeast septin organization from polarized fluorescence microscopy. Nature 2006;443:466–469. [PubMed: 17006515]
11. Lippincott J, Shannon KB, Shou W, Deshaies RJ, Li R. The Tem1 small GTPase controls actomyosin and septin dynamics during cytokinesis. J Cell Sci 2001;114:1379–1386. [PubMed: 11257003]
12. Rodal AA, Kozubowski L, Goode BL, Drubin DG, Hartwig JH. Actin and septin ultrastructures at the budding yeast cell cortex. Mol Biol Cell 2005;16:372–384. [PubMed: 15525671]

13. Fiala JC, Feinberg M, Popov V, Harris KM. Synaptogenesis via dendritic filopodia in developing hippocampal area CA1. J Neurosci 1998;18:8900–8911. [PubMed: 9786995]
14. Papa M, Segal M. Morphological plasticity in dendritic spines of cultured hippocampal neurons. Neuroscience 1996;71:1005–1011. [PubMed: 8684603]
15. Ziv NE, Smith SJ. Evidence for a role of dendritic filopodia in synaptogenesis and spine formation. Neuron 1996;17:91–102. [PubMed: 8755481]
16. Dailey ME, Smith SJ. The dynamics of dendritic structure in developing hippocampal slices. J Neurosci 1996;16:2983–2994. [PubMed: 8622128]
17. Parnass Z, Tashiro A, Yuste R. Analysis of spine morphological plasticity in developing hippocampal pyramidal neurons. Hippocampus 2000;10:561–568. [PubMed: 11075826]
18. Tada T, Sheng M. Molecular mechanisms of dendritic spine morphogenesis. Curr Opin Neurobiol 2006;16:95–101. [PubMed: 16361095]
19. Kusch J, Meyer A, Snyder MP, Barral Y. Microtubule capture by the cleavage apparatus is required for proper spindle positioning in yeast. Genes Dev 2002;16:1627–1639. [PubMed: 12101122]
20. Huisman SM, Bales OA, Bertrand M, Smeets MF, Reed SI, Segal M. Differential contribution of Bud6p and Kar9p to microtubule capture and spindle orientation in S. cerevisiae. J Cell Biol 2004;167:231–244. [PubMed: 15492045]
21. Grava S, Schaerer F, Faty M, Philippsen P, Barral Y. Asymmetric recruitment of dynein to spindle poles and microtubules promotes proper spindle orientation in yeast. Dev Cell 2006;10:425–439. [PubMed: 16580990]
22. Barral Y, Parra M, Bidlingmaier S, Snyder M. Nim1-related kinases coordinate cell cycle progression with the organization of the peripheral cytoskeleton in yeast. Genes Dev 1999;13:176–187. [PubMed: 9925642]
23. Shulewitz MJ, Inouye CJ, Thorner J. Hsl7 localizes to a septin ring and serves as an adapter in a regulatory pathway that relieves tyrosine phosphorylation of Cdc28 protein kinase in Saccharomyces cerevisiae. Mol Cell Biol 1999;19:7123–7137. [PubMed: 10490648]
24. Bi E, Maddox P, Lew DJ, Salmon ED, McMillan JN, Yeh E, Pringle JR. Involvement of an actomyosin contractile ring in Saccharomyces cerevisiae cytokinesis. J Cell Biol 1998;142:1301–1312. [PubMed: 9732290]
25. Roh DH, Bowers B, Schmidt M, Cabib E. The septation apparatus, an autonomous system in budding yeast. Mol Biol Cell 2002;13:2747–2759. [PubMed: 12181343]
26. DeMarini DJ, Adams AE, Fares H, De Virgilio C, Valle G, Chuang JS, Pringle JR. A septin-based hierarchy of proteins required for localized deposition of chitin in the Saccharomyces cerevisiae cell wall. J Cell Biol 1997;139:75–93. [PubMed: 9314530]
27. Barral Y, Mermall V, Mooseker MS, Snyder M. Compartmentalization of the cell cortex by septins is required for maintenance of cell polarity in yeast. Mol Cell 2000;5:841–851. [PubMed: 10882120]
28. Takizawa PA, DeRisi JL, Wilhelm JE, Vale RD. Plasma membrane compartmentalization in yeast by messenger RNA transport and a septin diffusion barrier. Science 2000;290:341–344. [PubMed: 11030653]
29. Bloodgood BL, Sabatini BL. Neuronal activity regulates diffusion across the neck of dendritic spines. Science 2005;310:866–869. [PubMed: 16272125]
30. Majewska A, Brown E, Ross J, Yuste R. Mechanisms of calcium decay kinetics in hippocampal spines: role of spine calcium pumps and calcium diffusion through the spine neck in biochemical compartmentalization. J Neurosci 2000;20:1722–1734. [PubMed: 10684874]
31. Hayashi Y, Majewska AK. Dendritic spine geometry: functional implication and regulation. Neuron 2005;46:529–532. [PubMed: 15944122]
32. Ashby MC, Maier SR, Nishimune A, Henley JM. Lateral diffusion drives constitutive exchange of AMPA receptors at dendritic spines and is regulated by spine morphology. J Neurosci 2006;26:7046–7055. [PubMed: 16807334]
33. Bloodgood BL, Sabatini BL. Ca(2+) signaling in dendritic spines. Curr Opin Neurobiol 2007;17:345–351. [PubMed: 17451936]
34. Sala C, Piech V, Wilson NR, Passafaro M, Liu G, Sheng M. Regulation of dendritic spine morphology and synaptic function by Shank and Homer. Neuron 2001;31:115–130. [PubMed: 11498055]

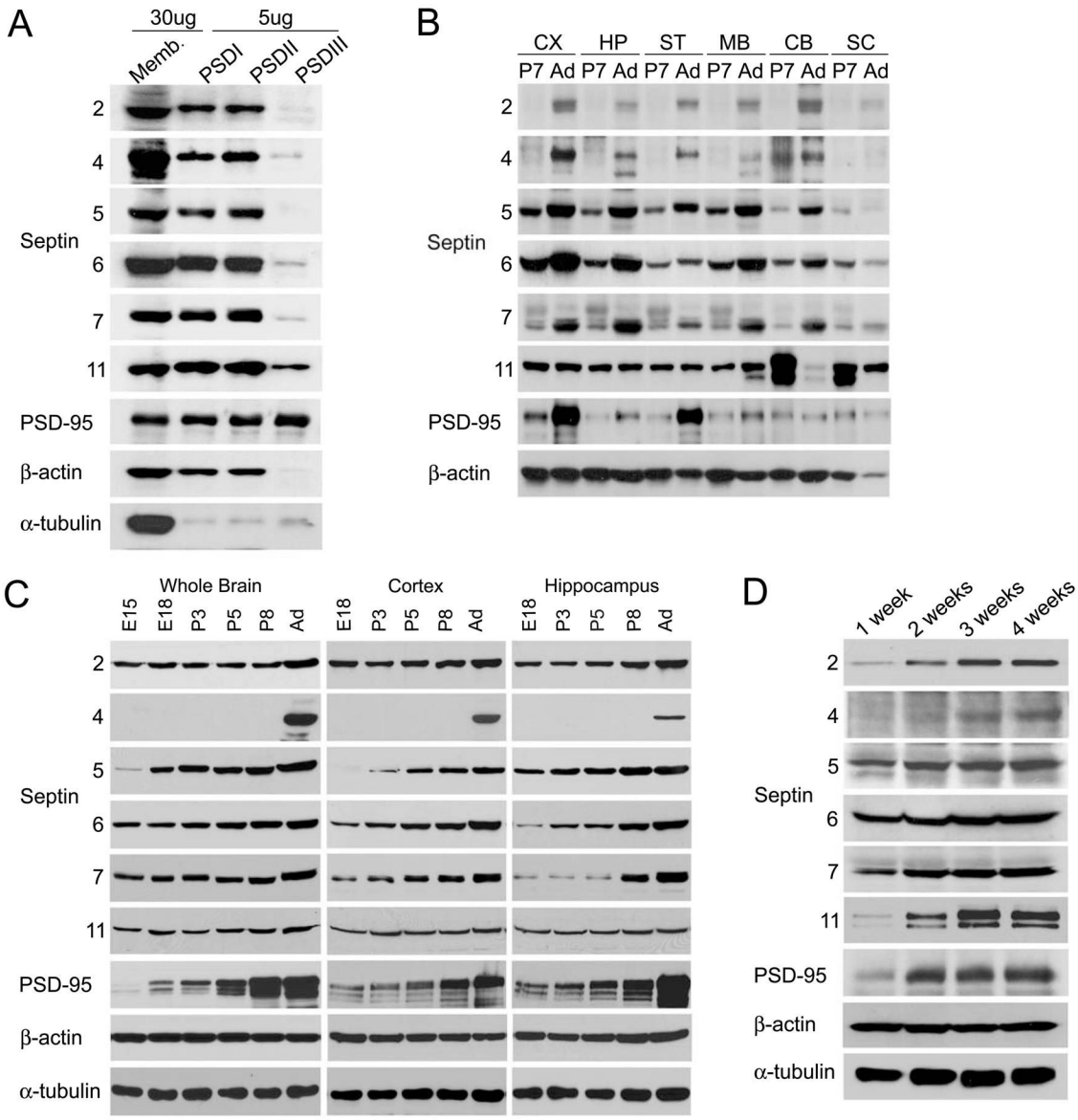

Figure 1. Expression pattern of septin family proteins in rat brain and hippocampal neuron culture

(A) Enrichment of septins in PSD preparation from adult rat forebrain. Crude synaptosomal membranes (P2) were prufied by discontinuous sucrose gradient and extracted with Triton X-100 once (PSD I), twice (PSD II), or with Triton X-100 followed by Sarkosyl (PSD III). PSD fractions (5 μg protein) were compared with 30 μg of crude synaptosomal membranes P2. (B) Regional distribution of septin proteins in the rat brain. Total homogenates (20 μg protein) from the indicated rat brain regions from P7 (postnatal day 7) and Ad (adult age; P45) animals were immunoblotted for the indicated proteins. CX: cortex, HP: hippocampus, ST: striatum, MB, midbrain, CB: cerebellum, SC: spinal cord. (C) Developmental expression pattern of septins in the rat brain. Immunoblot of total homogenates (20 μg protein) from the indicated rat brain regions at E15 (embryonic day 15), E18, P3, P5, P8 and Ad (P45). (D) Septin protein expression during development of dissociated hippocampal neurons in culture. Total extracts (15 μg) of hippocampal cultures at 1–4 weeks in vitro were immunoblotted as indicated.

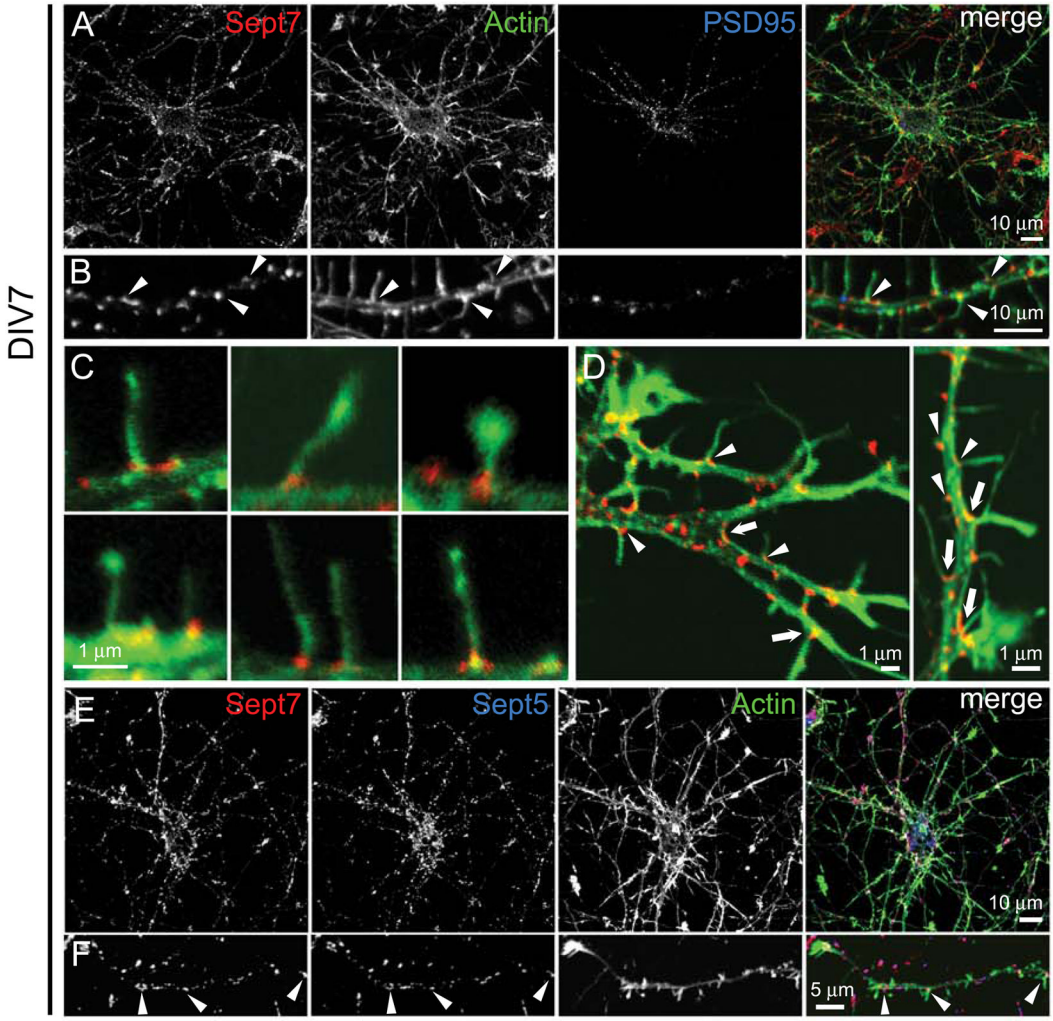

Figure 2. Endogenous Sept7 localization at the base of dendritic protrusions and dendritic branch points in cultured hippocampal neurons

(A–D) Cultured hippocampal neurons (DIV7) were fixed and immunostained for Sept7 (red), F-actin (phalloidin staining, green) and PSD-95 (blue). Low magnification images show whole neurons (A) and higher magnification images show dendrite segments (B). Arrowheads in B mark examples of Sept7 at the base of actin-rich dendritic protrusions. (C) High magnification merged images (actin, green; Sept7, red) showing examples of Sept7 localization at the base of individual protrusions. (D) Examples of Sept7 localization at dendritic branch points (arrows) and at the base of dendritic protrusions (arrowheads). (E and F) Endogenous Sept7 (red) were immunostained together with endogenous Sept5 (blue) and F-actin (green). Low magnification images show whole neurons (E) and higher magnification images show dendrite segments (F). Arrowheads indicate examples of colocalized Sept7 with Sept5 at the base of dendritic protrusions.

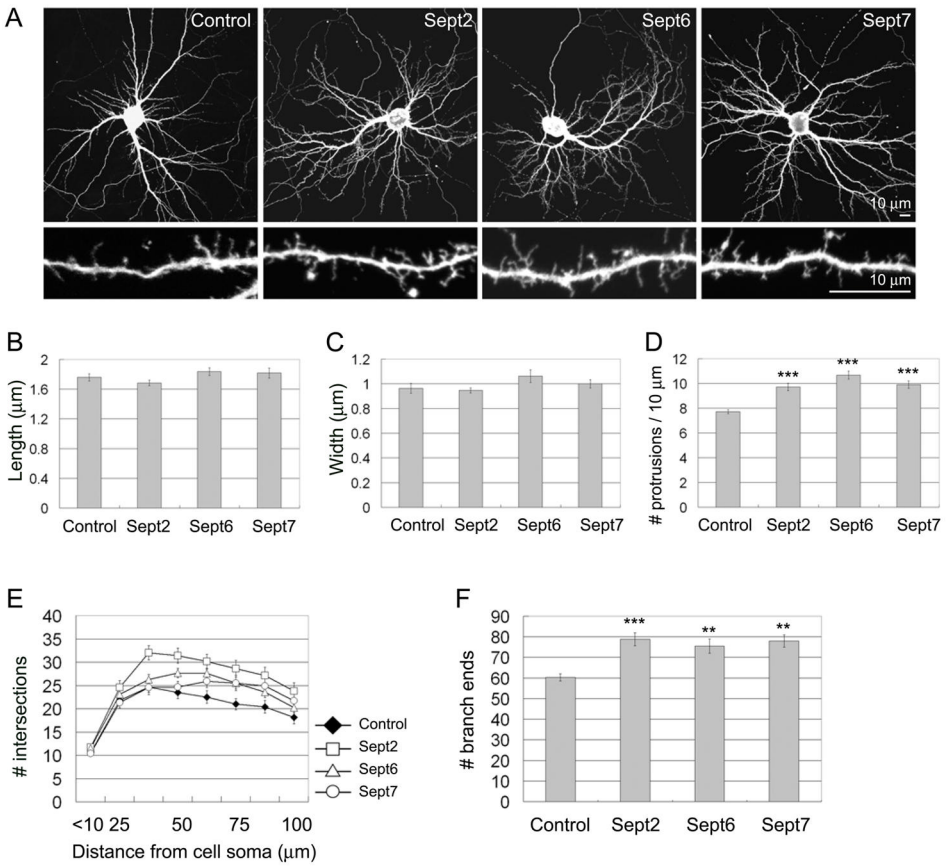

Figure 3. Septin overexpression increases dendritic protrusions and branches

(A) Cultured hippocampal neurons (DIV7) were transfected with the empty FLAG expression vector pFLAG-CMV-2, or FLAG-tagged Sept2, 6 or 7, as indicated. Neuron morphology was visualized by cotransfected EGFP. 5 days after transfection (DIV7+5), neurons were fixed and immunostained for EGFP and FLAG. (B–D) Average length (B), head width (C) and density (D) of dendritic protrusions in neurons transfected with the indicated constructs. (E) Dendrite complexity of neurons transfected with the indicated constructs measured by Sholl analysis, which shows the number of dendrites crossing circles (vertical axis) at various radial distances from the cell soma (horizontal axis). (F) Number of dendrite branch ends in hippocampal neurons transfected with the indicated constructs. Histograms show mean ± SEM; ***$p < 0.001$, ** $p < 0.01$, One-way ANOVA. n numbers for each condition were control FLAG (41), FLAG-Sept2 (34), FLAG-Sept6 (38) and FLAG-Sept7 (29).

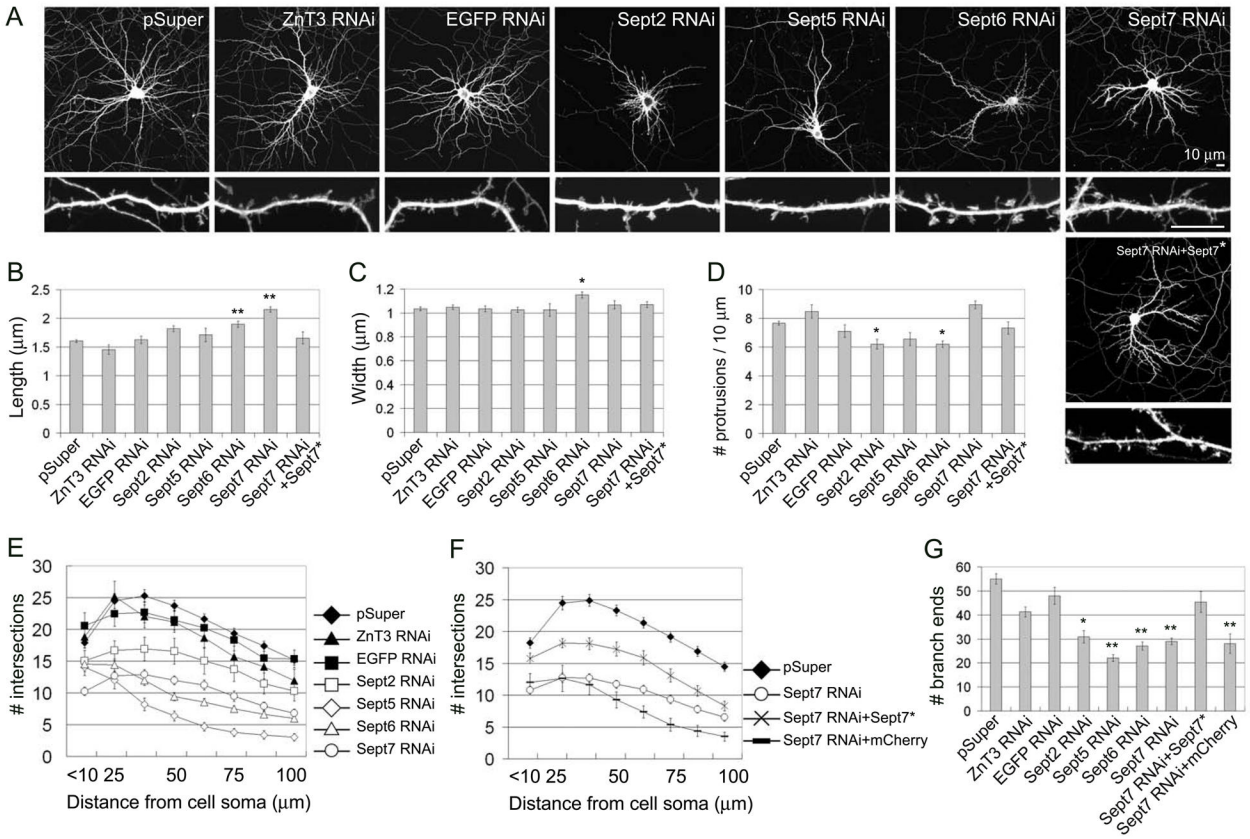

Figure 4. Effect of septin RNAi on dendritic protrusions and dendrite branching

(A) Cultured hippocampal neurons (DIV7) were transfected with empty expression vector pSuper, or with pSuper plasmids expressing ZnT3-shRNA (ZnT3 RNAi), EGFP-shRNA (EGFP RNAi), Sept2-shRNA (Sept2 RNAi), Sept5-shRNA (Sept5 RNAi), Sept6-shRNA (Sept6 RNAi), Sept7-shRNA (Sept7 RNAi), as indicated. For "rescue" experiments, Sept7-shRNA plasmid was cotransfected with RNAi-resistant Sept7 cDNA (Sept7 RNAi+Sept7*). 5 days after transfection (DIV7+5), neuron morphology was visualized by immunostaining for cotransfected β-gal. Scale bar, 10 μm (upper and lower panels). (B–D) Average length (B), head width (C) and density (D) of dendritic protrusions in neurons transfected with the indicated constructs. (E–G) Sholl analysis of dendrite branching (E and F) and branch end counts (G), as in Fig. 3. For a control of "rescue" experiments, mCherry plasmid was cotransfected with Sept7-shRNA (Sept7 RNAi+mCherry). Histograms show mean ± SEM; $^{**}p < 0.01$, $^{*}p < 0.05$, One-way ANOVA. n numbers for each condition were control pSuper (76), control ZnT3 RNAi (26), control EGFP RNAi (34), Sept2 RNAi (30), Sept5 RNAi (26), Sept6 RNAi (53), Sept7 RNAi (54), Sept7 RNAi+Sept7* (30), Sept7 RNAi+mCherry (30).